

# Highly Multiplexed Subcellular RNA Sequencing in Situ

Je Hyuk Lee,<sup>1,2\*</sup>† Evan R. Daugharthy,<sup>1,2,4\*</sup> Jonathan Scheiman,<sup>1,2</sup> Reza Kalhor,<sup>2</sup> Joyce L. Yang,<sup>2</sup> Thomas C. Ferrante,<sup>1</sup> Richard Terry,<sup>1</sup> Sauveur S. F. Jeanty,<sup>1</sup> Chao Li,<sup>1</sup> Ryoji Amamoto,<sup>3</sup> Derek T. Peters,<sup>3</sup> Brian M. Turczyk,<sup>1</sup> Adam H. Marblestone,<sup>1,2</sup> Samuel A. Inverso,<sup>1</sup> Amy Bernard,<sup>5</sup> Prashant Mali,<sup>2</sup> Xavier Rios,<sup>2</sup> John Aach,<sup>2</sup> George M. Church<sup>1,2†</sup>

<sup>1</sup>Wyss Institute, Harvard Medical School, Boston, MA 02115, USA. <sup>2</sup>Department of Genetics, Harvard Medical School, Boston, MA 02115, USA. <sup>3</sup>Department of Stem Cell and Regenerative Biology, Harvard University, Boston, MA 02138, USA. <sup>4</sup>Department of Systems Biology, Harvard Medical School, Boston, MA 02115, USA. <sup>5</sup>Allen Institute for Brain Science, Seattle, WA 98103, USA.

\* These authors contributed equally to this work.

†Corresponding author. E-mail: jehyuklee@mac.com (J.H.L.); gchurch@genetics.med.harvard.edu (G.M.C.)

**Understanding the spatial organization of gene expression with single-nucleotide resolution requires localizing the sequences of expressed RNA transcripts within a cell in situ. Here, we describe fluorescent in situ RNA sequencing (FISSEQ), in which stably cross-linked cDNA amplicons are sequenced within a biological sample. Using 30-base reads from 8742 genes in situ, we examined RNA expression and localization in human primary fibroblasts with a simulated wound-healing assay. FISSEQ is compatible with tissue sections and whole-mount embryos and reduces the limitations of optical resolution and noisy signals on single-molecule detection. Our platform enables massively parallel detection of genetic elements, including gene transcripts and molecular barcodes, and can be used to investigate cellular phenotype, gene regulation, and environment in situ.**

The spatial organization of gene expression can be observed within a single cell, tissue, and organism, but the existing RNA localization methods are limited to a handful of genes per specimen, making it costly and laborious to localize RNA transcriptome-wide (1–3). We originally proposed fluorescent in situ sequencing (FISSEQ) in 2003 and subsequently developed methods to sequence DNA amplicons on a solid substrate for genome and transcriptome sequencing (4–7); however, sequencing the cellular RNA in situ for gene expression profiling requires a spatially structured sequencing library and an imaging method capable of resolving the amplicons.

We report here the next generation of FISSEQ. To generate cDNA amplicons within the cell (fig. S1), RNA was reverse-transcribed in fixed cells with tagged random hexamers (fig. S2A). We incorporated aminoallyl deoxyuridine 5'-triphosphate (dUTP) during reverse transcription (RT) (fig. S2B) and refixed the cells using BS(PEG)9, an amine-reactive linker with a 4-nm spacer. The cDNA fragments were then circularized before rolling circle amplification (RCA) (fig. S2C), and BS(PEG)9 was used to cross-link the RCA amplicons containing aminoallyl dUTP (fig. S2, D and E). We found that random hexamer-primed RT was inefficient (fig. S3A), but cDNA circularization was complete within hours (fig. S3, B to D). The result was single-stranded DNA nanoballs 200 to 400 nm in diameter (fig. S4A), consisting of numerous tandem repeats of the cDNA sequence. BS(PEG)9 reduced non-specific probe binding (fig. S4B), and amplicons were highly fluorescent after probe hybridization (fig. S4C). As a result, the amplicons could be rehybridized many times, with minimal changes in their signal-to-noise ratio or position (fig. S4, D and E). Using SOLiD sequencing by ligation (fig. S5), the signal overlap over 27 consecutive sequencing reactions was ~600 nm in diameter (fig. S4F). In induced pluripotent stem (iPS)

cells, the amplicons counterstained subcellular structures, such as the plasma membrane, the nuclear membrane, the nucleolus, and the chromatin (Fig. 1A, fig. S6, and movies S1 to S3). We were able to generate RNA sequencing libraries in different cell types, tissue sections, and whole-mount embryos for three-dimensional (3D) visualization that spanned multiple resolution scales (Fig. 1, B and C).

High numerical aperture and magnification are essential for imaging RNA molecules in single cells (8–10), but many gene expression patterns are most efficiently detected in a low-magnification and wide-field mode, where it typically becomes difficult to distinguish single molecules because of the optical diffraction limit and low sensitivity (11). To obtain a spot density that is high enough to yield statistically significant RNA localization, and yet sufficiently low for discerning individual molecules, we developed partition sequencing, in which preextended sequencing primers are used to reduce the number of molecular sequencing reactions through random mismatches at the ligation site (Fig. 2A). Progressively longer sequencing primers result in exponential reduction of the observed density, and the sequencing primer can be changed during imaging

to detect amplicon pools of different density.

Fluorescence microscopy can be accompanied by tissue-specific artifacts and autofluorescence, which impede accurate identification of objects. If objects are nucleic acids, however, discrete sequences rather than the analog signal intensity can be used to analyze the image. For FISSEQ, putative nucleic acid sequences are determined for all pixels. The sequencing reads are then compared with reference sequences, and a null value is assigned to unaligned pixels. With a suitably long read length ( $L$ ), a large number of unique sequences ( $n$ ) can be used to identify transcripts or any other objects with a false-positive rate of approximately  $n/4^L$  per pixel. Because the intensity threshold is not used, even faint objects are registered on the basis of their sequence, whereas background noise, autofluorescence, and debris are eliminated (Fig. 2B).

We applied these concepts to sequence the transcription start site of inducible mCherry mRNA in situ, analogous to 5' rapid amplification of cDNA ends–polymerase chain reaction (RACE-PCR) (12). After RT and molecular amplification of the 5' end followed by fluorescent probe hybridization (fig. S7A), we quantified the concentration- and time-dependent mCherry gene expression in situ (fig. S7B). Using sequencing-by-ligation, we then determined the identity of 15 contiguous bases from each amplicon in situ, corresponding to the transcription start site (fig. S7C). When the sequencing reads were mapped to the vector sequence, 7472 (98.7%) amplicons aligned to the positive strand of mCherry, and 3967 (52.4%) amplicons mapped within two bases of the predicted transcription start site (fig. S7D).

We then sequenced the transcriptome in human primary fibroblasts in situ (Fig. 3A) and generated sequencing reads of 27 bases with a median per-base error rate of 0.64% (fig. S8). Using an automated analysis pipeline (fig. S9), we identified 14,960 amplicons with size >5 pixels,

representing 4171 genes, of which 12,495 (90.6%) amplicons mapped to the correct annotated strand (Fig. 3B, fig. S10, and table S1). We found that mRNA (43.6%) was relatively abundant even though random hexamers were used for RT (Fig. 3C). Ninety genes with the highest expression counts included fibroblast markers (13), such as fibronectin (*FNI*); collagens (*COL1A1*, *COL1A2*, *COL3A1*); matrix metalloproteinases and inhibitors (*MMP14*, *MMP2*, *TIMP1*); osteonectin (*SPARC*); stanniocalcin (*STC1*); and the bone morphogenesis-associated transforming growth factor (TGF)-induced protein (*TGFB1*), representing extracellular matrix, bone development, and skin development [Benjamini-Hochberg false discovery rate (FDR)  $<10^{-19}$ ,  $10^{-5}$ , and  $10^{-3}$ , respectively] (Fig. 3D) (14). We made Illumina sequencing libraries to compare FISSEQ to RNA-seq. Pearson's  $r$  correlation coefficient between RNA-seq and FISSEQ ranged from 0.52 to 0.69 ( $P < 10^{-16}$ ), excluding one outlier (*FNI*). For 853 genes with more than one observation, Pearson's  $r$  was 0.57 ( $P < 10^{-16}$ ), 0.47 ( $P < 10^{-16}$ ), and 0.23 ( $P < 10^{-3}$ ) between FISSEQ and RNA-seq from fibroblasts, lymphocytes, and iPS cells, respectively (Fig. 3E). When FISSEQ was compared with gene expression arrays, Pearson's  $r$  was as high as 0.73 ( $P < 10^{-16}$ ) among moderately expressed genes, whereas genes with low or high expression levels correlated poorly ( $r < 0.4$ ) (fig. S11). Highly abundant genes in RNA-seq and gene expression arrays were involved in translation and splicing (figs. S11 and S12), whereas such genes were underrepresented in FISSEQ. We examined 12,427 (83.1%) and 2,533 (16.9%) amplicons in the cytoplasm and nuclei, respectively, and found that nuclear RNA was 2.1 [95% confidence interval (CI) 1.9 to 2.3] times more likely to be noncoding ( $P < 10^{-16}$ ), and antisense mRNA was 1.8 [95% CI 1.7 to 2.0] times more likely to be nuclear ( $P < 10^{-16}$ ). We confirmed nuclear enrichment of *MALAT1* and *NEAT1* by comparing their relative distribution against all RNAs (Fig. 3F) or mitochondrial 16S ribosomal RNA (rRNA) (table S2), whereas mRNA such as *COL1A1*, *COL1A2*, and *THBS1* localized to the cytoplasm (table S3). We also examined splicing junctions of *FNI*, given its high read coverage (481 reads over 8.9 kb). *FNI* has three variable domains referred to as EDA, EDB, and IIICS, which are alternatively spliced (15). We did not observe development-associated EDB, but observed adult tissue-associated EDA and IIICS (Fig. 3G).

We also sequenced primary fibroblasts in situ after simulating a response to injury, obtaining 171,730 reads ( $>5$  pixels), representing 6880 annotated genes (Fig. 4A and fig. S13A to D). Pearson's  $r$  was 0.99 and 0.91 between different wound sites and growth conditions, respectively (Fig. 4B and fig. S13, E and F). In medium with epidermal growth factor (EGF), 81.6% of the amplicons were rRNA compared to 51.4% in fetal bovine serum (FBS) medium. When the 100 highest ranked genes were clustered, cells in FBS medium were enriched for fibroblast-associated GO terms, whereas rapidly dividing cells in EGF medium were less fibroblast-like (Fig. 4C) with alternative splicing of *FNI* (fig. S14). In regions containing migrating cells versus contact inhibited cells, 12 genes showed differences in relative gene expression (Fisher's exact test  $P < 0.05$  and  $>5$ -fold change) (Fig. 4, D to F, and table S4), eight of which were associated with the extracellular matrix (ECM)-receptor-cytoskeleton interaction, including *GID4*, *FHDC1*, *PRPF40A*, *LMO7*, and *WNK1* (Fig. 4G and table S4).

In summary, we present a platform for transcriptome-wide RNA sequencing in situ and demonstrate imaging and analytic approaches across multiple specimen types and spatial scales. FISSEQ correlates well with RNA-seq, except for genes involved in RNA and protein processing, possibly because some cellular structures or classes of RNA are less accessible to FISSEQ. It is notable that FISSEQ generates far fewer reads than RNA-seq but predominantly detects genes characterizing cell type and function. If this finding can be generalized, FISSEQ may be used to identify cell types based on gene expression profiles in situ. Using partition sequencing to control the signal density, it may even be possible to combine transcriptome profiling and in situ mutation detec-

tion in a high-throughput manner (16–18). Using RNA barcodes from expression vectors, one can label up to  $4^N$  ( $N$  = barcode length) cells uniquely, much more than is possible using a combination of fluorescent proteins (19). Similar to next-generation sequencing, we expect advances in read length, sequencing depth and coverage, and library preparation (i.e., fragmentation, rRNA depletion, targeted sequencing). Such advances may lead to improved stratification of diseased tissues in clinical medicine. While more work remains, our present demonstration is an important first step toward a new era in biology and medicine.

## References and Notes

1. G. Diez-Roux, S. Banfi, M. Sultan, L. Geffers, S. Anand, D. Rozado, A. Magen, E. Canidio, M. Pagani, I. Peluso, N. Lin-Marq, M. Koch, M. Bilio, I. Cantello, R. Verde, C. De Masi, S. A. Bianchi, J. Cicchini, E. Perroud, S. Mehmeti, E. Dagand, S. Schrunner, A. Nürnberger, K. Schmidt, K. Metz, C. Zwingmann, N. Brieske, C. Springer, A. M. Hernandez, S. Herzog, F. Grabbe, C. Sieverding, B. Fischer, K. Schrader, M. Brockmeyer, S. Dettmer, C. Helbig, V. Alunni, M. A. Battaini, C. Mura, C. N. Henrichsen, R. Garcia-Lopez, D. Echevarria, E. Puelles, E. Garcia-Calero, S. Kruse, M. Uhr, C. Kauck, G. Feng, N. Milyaev, C. K. Ong, L. Kumar, M. Lam, C. A. Semple, A. Gyenesi, S. Mundlos, U. Radelof, H. Lehrach, P. Sarmientos, A. Reymond, D. Davidson, P. Dollé, S. E. Antonarakis, M. L. Yaspo, S. Martinez, R. A. Baldock, G. Eichele, A. Ballabio, A high-resolution anatomical atlas of the transcriptome in the mouse embryo. *PLoS Biol.* **9**, e1000582 (2011). [Medline doi:10.1371/journal.pbio.1000582](https://doi.org/10.1371/journal.pbio.1000582)
2. H. Zeng, E. H. Shen, J. G. Hohmann, S. W. Oh, A. Bernard, J. J. Royall, K. J. Glattfelder, S. M. Sunkin, J. A. Morris, A. L. Guillozet-Bongaarts, K. A. Smith, A. J. Ebbert, B. Swanson, L. Kuan, D. T. Page, C. C. Overly, E. S. Lein, M. J. Hawrylycz, P. R. Hof, T. M. Hyde, J. E. Kleinman, A. R. Jones, Large-scale cellular-resolution gene profiling in human neocortex reveals species-specific molecular signatures. *Cell* **149**, 483–496 (2012). [Medline doi:10.1016/j.cell.2012.02.052](https://doi.org/10.1016/j.cell.2012.02.052)
3. E. Lécuyer, H. Yoshida, N. Parthasarathy, C. Alm, T. Babak, T. Cerovina, T. R. Hughes, P. Tomancak, H. M. Krause, Global analysis of mRNA localization reveals a prominent role in organizing cellular architecture and function. *Cell* **131**, 174–187 (2007). [Medline doi:10.1016/j.cell.2007.08.003](https://doi.org/10.1016/j.cell.2007.08.003)
4. J. Shendure, G. J. Porreca, N. B. Reppas, X. Lin, J. P. McCutcheon, A. M. Rosenbaum, M. D. Wang, K. Zhang, R. D. Mitra, G. M. Church, Accurate multiplex polony sequencing of an evolved bacterial genome. *Science* **309**, 1728–1732 (2005). [Medline doi:10.1126/science.1117389](https://doi.org/10.1126/science.1117389)
5. J. B. Kim, G. J. Porreca, L. Song, S. C. Greenway, J. M. Gorham, G. M. Church, C. E. Seidman, J. G. Seidman, Polony multiplex analysis of gene expression (PMAGE) in mouse hypertrophic cardiomyopathy. *Science* **316**, 1481–1484 (2007). [Medline doi:10.1126/science.1137325](https://doi.org/10.1126/science.1137325)
6. R. D. Mitra, V. L. Butty, J. Shendure, B. R. Williams, D. E. Housman, G. M. Church, Digital genotyping and haplotyping with polymerase colonies. *Proc. Natl. Acad. Sci. U.S.A.* **100**, 5926–5931 (2003). [Medline doi:10.1073/pnas.0936399100](https://doi.org/10.1073/pnas.0936399100)
7. R. Drmanac, A. B. Sparks, M. J. Callow, A. L. Halpern, N. L. Burns, B. G. Kermani, P. Carnevali, I. Nazarenko, G. B. Nilsen, G. Yeung, F. Dahl, A. Fernandez, B. Staker, K. P. Pant, J. Baccash, A. P. Borcharding, A. Brownley, R. Cedeno, L. Chen, D. Chernikoff, A. Cheung, R. Chirita, B. Curson, J. C. Ebert, C. R. Hacker, R. Hartlage, B. Hauser, S. Huang, Y. Jiang, V. Karpinchyk, M. Koenig, C. Kong, T. Landers, C. Le, J. Liu, C. E. McBride, M. Morenzoni, R. E. Morey, K. Mutch, H. Perazich, K. Perry, B. A. Peters, J. Peterson, C. L. Pethiyagoda, K. Pothuraju, C. Richter, A. M. Rosenbaum, S. Roy, J. Shafit, U. Sharanovich, K. W. Shannon, C. G. Sheppy, M. Sun, J. V. Thakuria, A. Tran, D. Vu, A. W. Zaranek, X. Wu, S. Drmanac, A. R. Oliphant, W. C. Banyai, B. Martin, D. G. Ballinger, G. M. Church, C. A. Reid, Human genome sequencing using unchained base reads on self-assembling DNA nanoarrays. *Science* **327**, 78–81 (2010). [Medline doi:10.1126/science.1181498](https://doi.org/10.1126/science.1181498)
8. A. M. Femino, F. S. Fay, K. Fogarty, R. H. Singer, Visualization of single RNA transcripts in situ. *Science* **280**, 585–590 (1998). [Medline doi:10.1126/science.280.5363.585](https://doi.org/10.1126/science.280.5363.585)
9. J. M. Levisky, S. M. Shenoy, R. C. Pezo, R. H. Singer, Single-cell gene expression profiling. *Science* **297**, 836–840 (2002). [Medline doi:10.1126/science.1072241](https://doi.org/10.1126/science.1072241)

10. A. Raj, P. van den Bogaard, S. A. Rifkin, A. van Oudenaarden, S. Tyagi, Imaging individual mRNA molecules using multiple singly labeled probes. *Nat. Methods* **5**, 877–879 (2008). [Medline doi:10.1038/nmeth.1253](#)
11. S. Itzkovitz, A. van Oudenaarden, Validating transcripts with probes and imaging technology. *Nat. Methods* **8** (Suppl), S12–S19 (2011). [Medline doi:10.1038/nmeth.1573](#)
12. M. A. Frohman, M. K. Dush, G. R. Martin, Rapid production of full-length cDNAs from rare transcripts: Amplification using a single gene-specific oligonucleotide primer. *Proc. Natl. Acad. Sci. U.S.A.* **85**, 8998–9002 (1988). [Medline doi:10.1073/pnas.85.23.8998](#)
13. R. J. McNulty, Fibroblasts and myofibroblasts: Their source, function and role in disease. *Int. J. Biochem. Cell Biol.* **39**, 666–671 (2007). [Medline doi:10.1016/j.biocel.2006.11.005](#)
14. W. Huang, B. T. Sherman, R. A. Lempicki, Systematic and integrative analysis of large gene lists using DAVID bioinformatics resources. *Nat. Protoc.* **4**, 44–57 (2009). [Medline doi:10.1038/nprot.2008.211](#)
15. A. R. Kornblihtt, C. G. Pesce, C. R. Alonso, P. Cramer, A. Srebrow, S. Werbajh, A. F. Muro, The fibronectin gene as a model for splicing and transcription studies. *FASEB J.* **10**, 248–257 (1996). [Medline](#)
16. R. Ke, M. Mignardi, A. Pacureanu, J. Svedlund, J. Botling, C. Wählby, M. Nilsson, In situ sequencing for RNA analysis in preserved tissue and cells. *Nat. Methods* **10**, 857–860 (2013). [Medline doi:10.1038/nmeth.2563](#)
17. K. Zhang, J. B. Li, Y. Gao, D. Egli, B. Xie, J. Deng, Z. Li, J. H. Lee, J. Aach, E. M. Leproust, K. Eggan, G. M. Church, Digital RNA allelotyping reveals tissue-specific and allele-specific gene expression in human. *Nat. Methods* **6**, 613–618 (2009). [Medline doi:10.1038/nmeth.1357](#)
18. J. H. Lee, I. H. Park, Y. Gao, J. B. Li, Z. Li, G. Q. Daley, K. Zhang, G. M. Church, A robust approach to identifying tissue-specific gene expression regulatory variants using personalized human induced pluripotent stem cells. *PLoS Genet.* **5**, e1000718 (2009). [Medline doi:10.1371/journal.pgen.1000718](#)
19. J. Livet, T. A. Weissman, H. Kang, R. W. Draft, J. Lu, R. A. Bennis, J. R. Sanes, J. W. Lichtman, Transgenic strategies for combinatorial expression of fluorescent proteins in the nervous system. *Nature* **450**, 56–62 (2007). [Medline doi:10.1038/nature06293](#)

**Acknowledgments:** Data can be downloaded from [www.arep.med.harvard.edu/FISSEQ\\_Science\\_2014/](http://www.arep.med.harvard.edu/FISSEQ_Science_2014/) and Gene Expression Omnibus (gene expression arrays: GSM313643, GSM313646, and GSM313657; RNA-seq: GSE54733). We thank S. Kosuri, K. Zhang, and M. Nilsson for discussions; A. DePace for *Drosophila* embryos; and I. Bachelet for antibody conjugation. Funded by NIH Centers of Excellence in Genomic Sciences grant P50 HG005550. J.H.L. and co-workers were funded by National Heart, Lung, and Blood Institute, NIH, grant RC2HL102815; Allen Institute for Brain Science, and National Institute of Mental Health, NIH, grant MH098977. E.R.D. was funded by NIH grant GM080177 and NSF Graduate Research Fellowship Program grant DGE1144152. A.H.M. funded by the Hertz Foundation. Potential conflicts of interests for G.M.C. are listed on <http://arep.med.harvard.edu/gmc/tech.html>. J.H.L., E.D., R.T., and G.M.C. are authors on a patent application from the Wyss Institute that covers the method of generating three-dimensional nucleic acid-containing matrix.

#### Supplementary Materials

[www.sciencemag.org/cgi/content/full/science.1250212/DC1](http://www.sciencemag.org/cgi/content/full/science.1250212/DC1)

Materials and Methods

Supplementary Text

Figs. S1 to S14

Tables S1 to S4

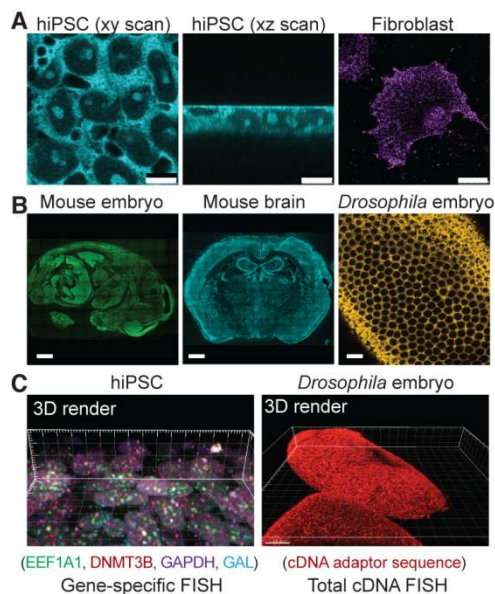
Movies S1 to S6

References

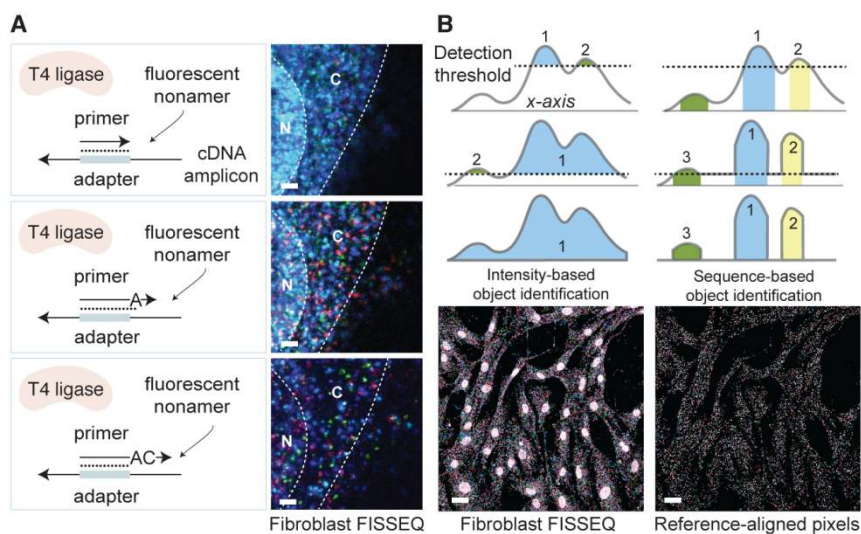
26 December 2013; accepted 13 February 2014

Published online 27 February 2014; 10.1126/science.1250212



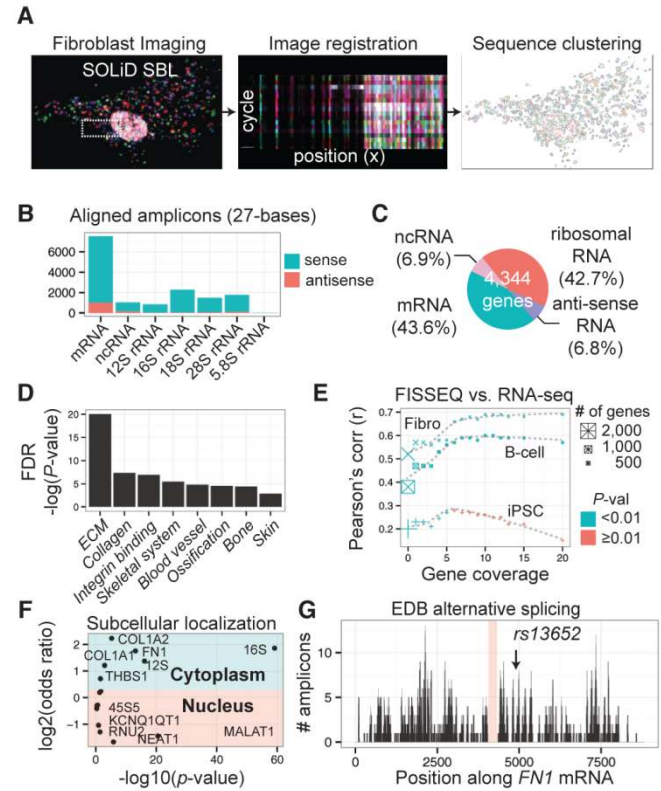


**Fig. 1. Construction of 3D RNA-seq libraries in situ.** After RT using random hexamers with an adapter sequence in fixed cells, the cDNA is amplified and cross-linked in situ. **(A)** A fluorescent probe is hybridized to the adapter sequence and imaged by confocal microscopy in human iPS cells (hiPSC) (scale bar: 10  $\mu$ m) and fibroblasts (scale bar: 25  $\mu$ m). **(B)** FISSEQ can localize the total RNA transcriptome in mouse embryo and adult brain sections (scale bar: 1 mm), and whole-mount *Drosophila* embryos (scale bar: 5  $\mu$ m), although we have not sequenced these samples. **(C)** 3D rendering of gene-specific or adapter-specific probes hybridized to cDNA amplicons. FISH, fluorescence in situ hybridization.



**Fig. 2. Overcoming resolution limitations and enhancing the signal-to-noise ratio.** **(A)** Ligation of fluorescent oligonucleotides occurs when the sequencing primer ends are perfectly complementary to the template. Extending sequencing primers by one or more bases, one can randomly sample amplicons at 1/4th, 1/16th, and 1/256th of the original density in fibroblasts (scale bar: 5  $\mu$ m). N, nucleus; C, cytoplasm. **(B)** Rather than using an arbitrary intensity threshold, color sequences at each pixel are used to identify objects. For sequences of  $L$  bases, the error rate is approximately  $n/4^L$  per pixel, where  $n$  is the size of the reference. By removing unaligned pixels, the nuclear background noise is reduced in fibroblasts (scale bar: 20  $\mu$ m).

**Fig. 3. Whole-transcriptome in situ RNA-seq in primary fibroblasts.** (A) From deconvolved confocal images, 27-base reads are aligned to the reference, and alignments are spatially clustered into objects. (B) Of the amplicons, 90.6% align to the annotated (+) strand. (C) mRNA and noncoding RNA make up 43.6% and 6.9% of the amplicons, respectively. (D) GO term clustering for the top 90 ranked genes. (E) FISSEQ of 2710 genes from fibroblasts compared with RNA-seq for fibroblast, B cell, and iPSC cells. Pearson's correlation is plotted as a function of the gene expression level. (F) Subcellular localization enrichment compared to the whole transcriptome distribution. (G) Of the amplicons, 481 map to the *FN1* mRNA, showing an alternatively spliced transcript variant and a single-nucleotide polymorphism (arrow).



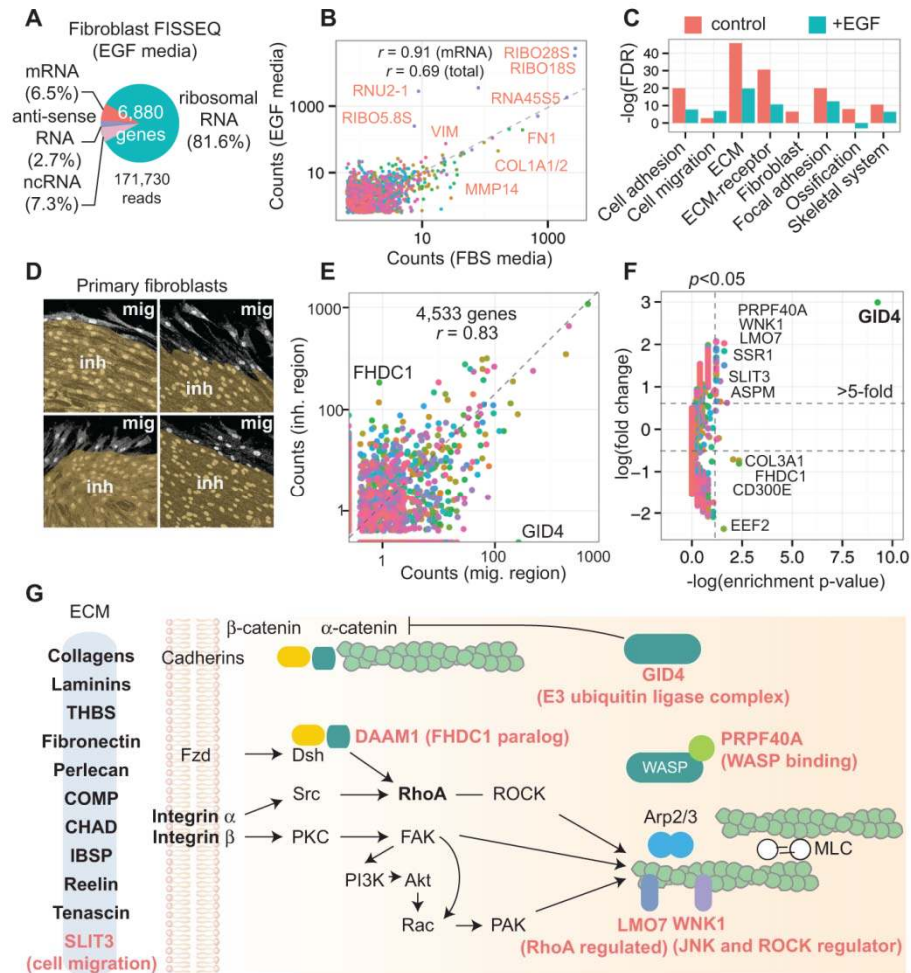


**Fig. 4. Functional analysis of fibroblasts during simulated wound healing.** (A) In EGF medium, rRNA makes up 81.6% of the amplicons. (B) EGF medium 109,646 reads compared with 14,960 reads from FBS medium (different colors denote genes). (C) Top 100 ranked genes from FBS versus EGF FISSEQ clustered for functional annotation. (D) An in vitro wound-healing assay allows cells to migrate (mig) into the wound gap. inh, contact-inhibited cells. The image segments are based on the cell morphology. (E) Comparison of 4,533 genes from migrating and contact-inhibited cells. (F) Twelve genes are differentially expressed (Fisher's exact test  $P < 0.05$  and >fivefold; 180 genes). (See table S4.) (G) Top 100 genes in fibroblasts are enriched for terms associated with ECM-receptor interaction and focal adhesion kinase complex (bold letters). During cell migration, genes involved in ECM-receptor-cytoskeleton signaling and remodeling are differentially expressed (red letters). THBS, thrombospondin; COMP, cartilage oligomeric matrix protein; CHAD, chondroadherin; IBSP, integrin-binding sialoprotein; PKC, protein kinase C; FAK, focal adhesion kinase; PI3K, phosphatidylinositol 3-kinase; MLC, myosin light chain; PAK, p21-activated protein kinase.